CONTACT ANALYSIS AND SIMULATION OF ROLLED PLASTIC FILM USED FOR ROOF VENTILATION IN JAPANESE GREENHOUSES

N. A. Noda, L. Wang, H. Nagatomo, Y. Sano, Y. Takase

ABSTRACT. *Greenhouses are capable of producing a variety of high-value crops year-round. A novel Japanese greenhouse design is gaining popularity because of its automated roll-up ventilation system that is integrated into the roof. However, due to the frequent movement of the roll-up system, the plastic film deteriorates rapidly and typically lasts for only three or four months. In order to better understand the film deterioration, we studied the mechanics involved at the point of contact between the film and the metal greenhouse frame. We found that film deformation and failure were closely related to stretching and creasing, and these processes were observed at the microscopic level. An experimental device was developed to further study the damage to greenhouse film due to the roll-up movement. We concluded that the reduction in film thickness due to static loading or rolling contact was the best predictor of future film damage.*

Keywords. *Compression, Finite element method analysis, Friction and wear, Polymer materials.*

Fully controlled plant production systems offer the possibility of providing a large number of high-quality crops with greater predictability. High crop quality can be achieved by an efficient structure such as a well-designed greenhouse, and covering materials for greenhouses can have a great impact on crop production. In the U.S., polyethylene (PE) film is the most common covering material for greenhouses, and in Europe, glass is typically used as covering material. In Japan, polyvinyl chloride (PVC) film is typically used as a single-layer covering material, and in 1985 a total area of 84,000 acres was covered this way (Giacomelli and Roberts, 1993; Takakura, 1988). However, in recent years, agricultural polyolefin (PO) film started to be used in Japan. Agricultural PO film is often used as a single multi-layered film laminated with PE and ethylene vinyl acetate copolymer (EVA) and coated with an anti-condensation drip layer that can prevent water droplets from forming on the film. These water droplets can fall onto the crop and cause tissue damage. Because agricultural PO film has high tensile strength, heat retention capabilities (blocking infrared radiation), and can be manufactured with an anti-condensation drip layer, agricultural PO films are quickly replacing PVC films in Japan (Sakaya et al., 2005). However, agricultural PO film still tears easily after repeated stress applications, e.g., from rubbing against the greenhouse structure (Nihon Nougyou System, 2014).

Traditional Japanese greenhouse designs are not always capable of adequately controlling summer temperatures, resulting in reduced flowering in strawberries and shorter harvest windows for cucumbers (Miyazaki, 2012). To solve these challenges, open-roof greenhouses are being developed, and some Japanese manufacturers have designed roofs that open and close with rolling plastic film. For these types of open-roof greenhouses, full or partial openings and automatic ventilation systems have been proposed. However, among these designs, the fully opening, automatically ventilated greenhouse, as shown in figure 1, has proven the most effective design that can adjust the inside temperature by automatically opening and closing the roof.

Figure 1 shows that the plastic film can be rolled up from the gutter toward the ridge. This ventilation system has been adopted in a large number of Japanese greenhouses. The roof typically opens partially so that the natural ventilation capacity is limited but sufficient for most crops. Holding straps can be used to control film flapping due to wind (fig. 2). In these greenhouses, the roof opens and closes frequently to adjust the greenhouse temperature automatically. Over time, this causes tearing of the film, resulting in a maximum lifespan of three to four months. Because plastic film can typically be used for two years in regular greenhouses, it is desirable to prolong the film life.

In this article, we examine film damage as a result of frequent movement for temperature control. We used the finite element method (FEM) to evaluate the stress and deformation of the plastic film. In addition, contact experiments were conducted to evaluate the damage of the film. Finally, results from the contact experiments and the FEM simulations were compared for four different agricultural PO films. Few previous studies are available that examine the damage of plastic films under rolling contact loading, and observa-

Submitted for review in July 2016 as manuscript number PAFS 12018; approved for publication by the Plant, Animal, & Facility Systems Community of ASABE in July 2016.

The authors are **Nao-Aki Noda,** Professor, **Luyu Wang,** Graduate Student, **Hiroyuki Nagatomo,** Graduate Student, **Yoshikazu Sano,** Senior Research Editor, and **Yasushi Takase,** Senior Research Associate, Department of Mechanical Engineering, Kyushu Institute of Technology, Fukuoka, Japan. **Corresponding author:** Nao-Aki Noda, Kyushu Institute of Technology, 1-1 Sensui-cho, Tobata-ku, Kitakyushu-shi, Fukuoka 804-8550, Japan; phone: +81-93-884-3124; e-mail: noda@mech.kyutech.ac.jp.

Vol. 59(5): 1421-1437 ISSN 2151-0032 DOI 10.13031/trans.59.12018

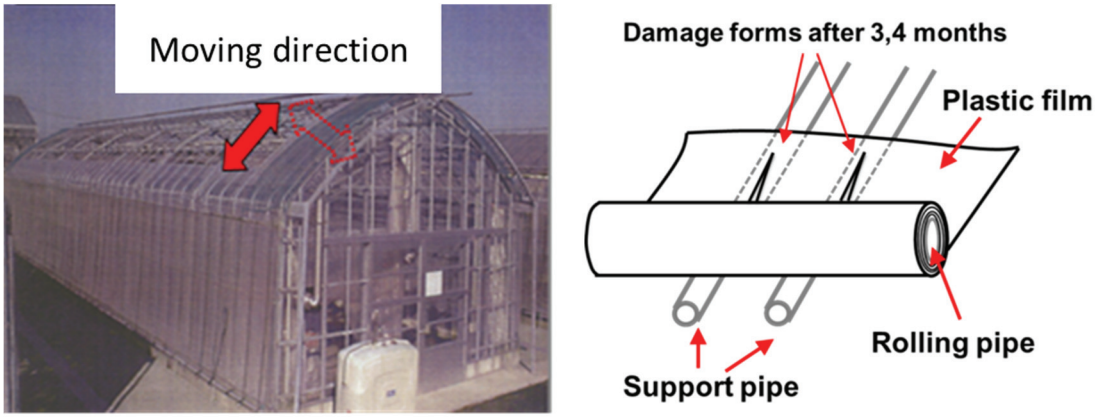

Figure 1. (a) Greenhouse with fully opening roof to control the inside temperature automatically and (b) illustration of an automatic roll-up system that uses a pipe and motor to roll the roof covering film.

Figure 2. (a) Greenhouse with fully opening roof and (b) straps used to hold the plastic film and roll-up system in place.

tions are typically reported for actual greenhouse installations (fig. 3).

Assumed Damage Process

Observations of Damaged Plastic Film

Figure 3 shows damaged plastic film (type B) after three months of use. The film was installed at the gutter side of the roof. The pressure on the film was largest when a small amount of film was rolled onto the pipe. Therefore, the film was most easily damaged at the gutter side of the roof, where the rolling pipe begins to roll the film up. Figures 3b and 3c show the top part of a tear with many creases and a line scar. The line scar develops at a crease and is the initial stage of damage. These line scars later merge into more significant damage. Figure 3d shows a close-up of serious film damage at the bottom of a significant tear that developed in the direction of movement of the roll-up pipe. We inferred that the line scar shown in figure 3c was formed due to compressive deformation and friction from the roll-up pipe. The formation of a scar is typical of initial film damage.

Figure 4 shows scanning electron microscope (SEM) images of the outside and inside surfaces of the film. No significant damage can be observed in figures 4a and 4b, but relatively rough surfaces are shown in figures 4c and 4d.

Figure 5 shows a roughness testing machine that can measure the surface roughness along a direction perpendicular to the rolling direction. Figure 5b shows the roughness measured on the outside surface of the film, and figure 5c shows the roughness measured on the inside surface of the film (Japanese Industrial Standards, 1994). It was found that the maximum roughness, as defined in JIS-B0601 (Japanese Industrial Standards, 1994), on the inside film surface (R_y = 11.6 μm) was approximately twice as large as the maximum roughness on the outside film surface (R_y = 5.1 μm). From figures 4 and 5, it can be concluded that film damage first occurs on the inside film surface due to contact between the film and the pipes of the greenhouse frame.

Assumed Damage Process from Observations

Figure 6 illustrates the damage process assumed from the observations shown in figures 3, 4, and 5. Figure 6a shows an intact film. After being subjected to compressive rolling, rolling indentations and stretched zones are formed. These stretched zones lead to several creases (fig. 6b). Next, the creases are folded over and develop into line scars (fig. 6c). The damage first occurs on the film surface that is in contact with the pipes of the greenhouse frame. Moreover, line scars

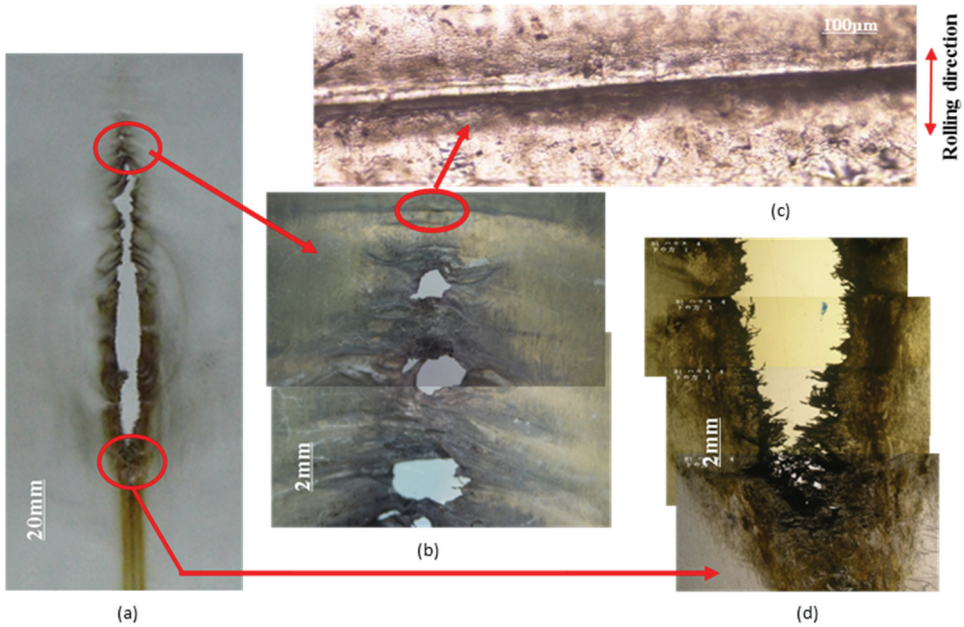

Figure 3. Damage observed on the inside surface of plastic film (type B) using a microscope: (a) torn film, (b) line scar development, (c) close-up of line scar, and (d) damage at the bottom of the tear.

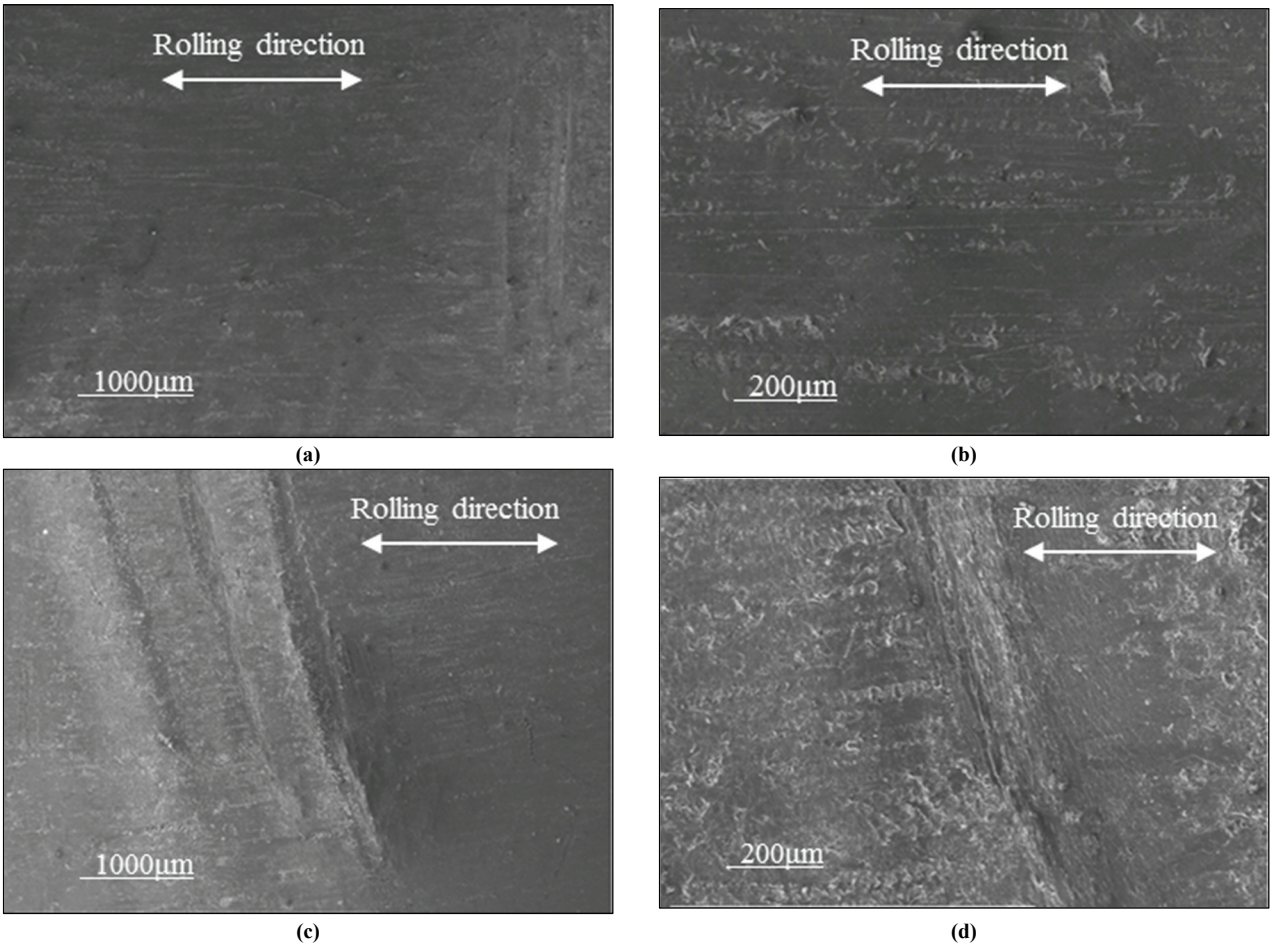

Figure 4. Film (type B) damage observed by scanning electron microscope: (a) and (b) outside film surface; (c) and (d) inside film surface.

develop perpendicular to the rolling direction (fig. 6d). Finally, the plastic film breaks and splits, as shown in figure 6e. We believe that several factors, such as the amount of deformation of the plastic film, the temperature of the frame pipes, and the roughness of the frame pipes, all affect the amount of damage to the plastic film.

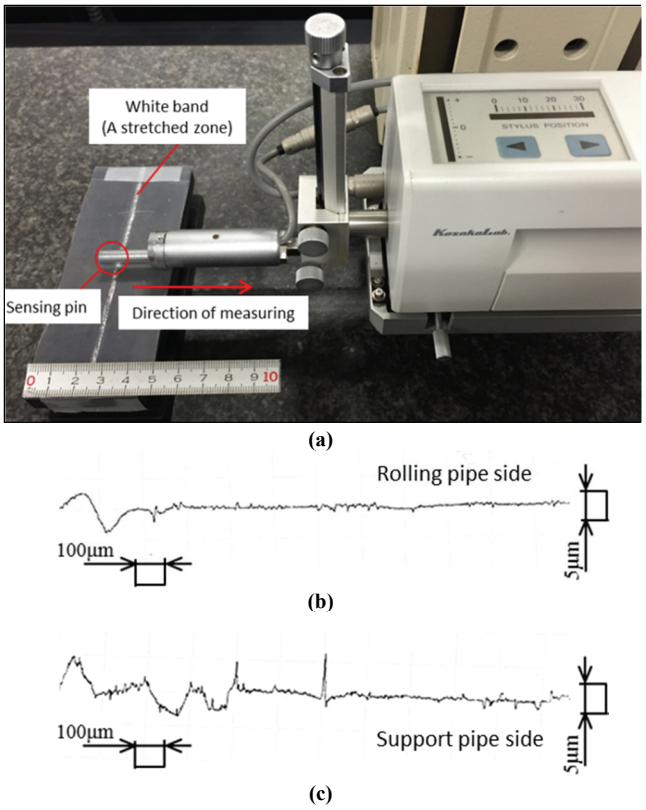

Figure 5. (a) Roughness testing machine used to measure surface roughness of film (type B) after 300 cycles of pipe rolling perpendicular to the rolling direction, (b) maximum roughness (R_y = 5.1 μm) measured on the outside surface of the film, and (c) maximum roughness (R_y = 11.6 μm) measured on the inside surface of the film (Japanese Industrial Standards, 1994).

STRESS-STRAIN RELATIONSHIPS

TENSILE TEST METHOD

The tensile tests and rolling contact experiments were conducted on plastic films and pipes. These materials are commonly used in greenhouse construction and were provided by the Miyazaki Agricultural Research Institute. The plastic film, which is made from low-density polyethylene (LDPE) or ethylene-vinyl acetate (EVA) copolymer, was produced by the inflation molding method. Tensile tests were conducted on four typical agricultural PO films made by different companies, herein referred to as types A, B, C, and D. All four films have the same thickness (t_0 = 0.15 mm) and consist of multiple laminated layers. The manufacturing details of the film were not provided by the manufacturers, so they are not listed. As an example, the results for film type B, which is used in the greenhouses of the Miyazaki Agricultural Research Institute, are presented in table 2, tables 4 through 6, figures 3 through 5, figures 11 through 14, figures 16 through 20, and figures 25 through 28. The pipes are hot-dip galvanized pipes corresponding to JIS-G3314 (Japanese Industrial Standards, 2010).

To analyze the deformation and stress of the film between the pipes, the stress-strain relationship of the plastic film was tested at two temperatures: 20°C ±1.5°C (ambient temperature) and 70°C (the maximum measured summer temperature of greenhouse pipe surfaces in Miyazaki Prefecture, Japan). The tensile test was conducted at 70°C using a heating lamp. Stress-strain curves were obtained over the 0% to 100% strain range. The dimensions of the plastic film used for the tensile test are prescribed in JIS-K7127 (Japanese Industrial Standards, 1999); however, to maintain a uniform temperature of 70°C ±2°C over the entire test piece, the length was shortened to 60 mm (fig. 7a). Breakage and slippage of the test piece from the chuck was suppressed by hard rubber inserted into the chuck, which exerted almost uniform pressure on the test piece. Although the strain rate in the tensile test ($\dot{\varepsilon}$ = 0.05 s^{-1}) differed from that at the rolling contact ($\dot{\varepsilon}$ = 5 s^{-1}), the stress-strain relationships in the two situations should vary by less than 10% (Tanimura et al., 2011).

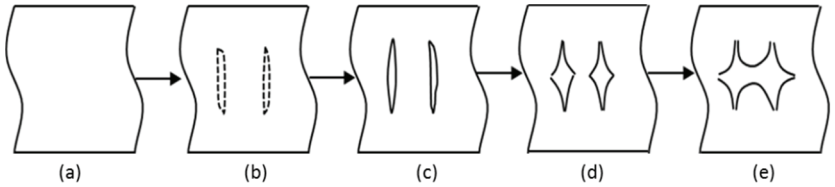

Figure 6. Predicted damage progression in greenhouse film. The damage first occurs on the inside surface of the film that is in contact with the pipes of the greenhouse frame. In this illustration, the film is rolled in the horizontal direction: (a) intact plastic film, (b) crease formation, (c) line scar formation, (d) line scar development, and (e) broken and split.

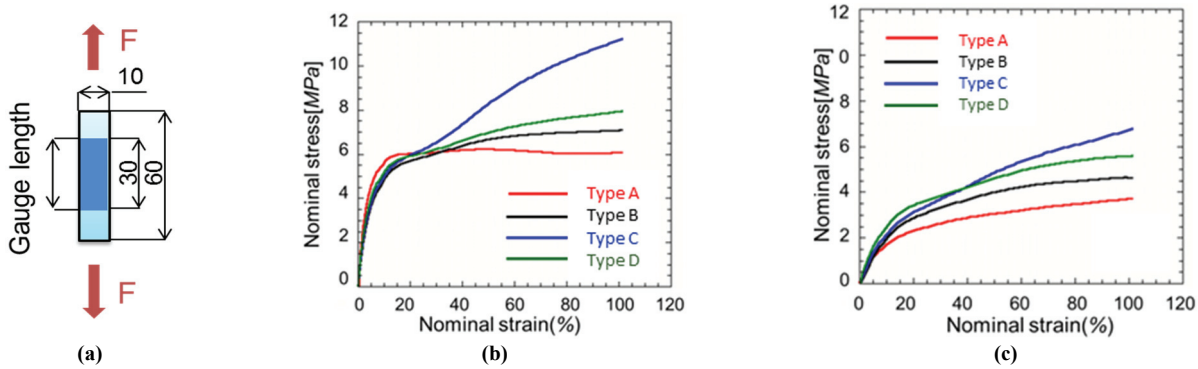

Figure 7. (a) Test piece geometry and stress-strain diagrams for different agricultural PO films at (b) T = 20°C, and (c) and T = 70°C.

Table 1. 60% offset yield strength obtained from figure 7.

Film	$\sigma_{60\%}$ at T = 20°C (MPa)	$\sigma_{60\%}$ at T = 70°C (MPa)	$\sigma_{60\%}$ at 70°C/ $\sigma_{60\%}$ at 20°C
Type A	6.2	3.2	0.52
Type B	6.8	4.3	0.62
Type C	9.2	5.4	0.58
Type D	7.3	5.0	0.68

Tensile Test Results

Stress-strain diagrams collected at room temperature (20°C) and 70°C are shown in figures 7b and 7c, respectively. For materials such as aluminum alloys, which exhibit no clear yield point, an offset yield strength ($\sigma_{0.2}$), set to 0.2% of the strain, is applied. In this study, because the film strain appears in the range 50% to 60% (see fig. 29a), $\sigma_{0.2}$ is replaced with a similarly defined quantity called the 60% offset yield strength ($\sigma_{60\%}$). Table 1 shows the 60% offset yield strength ($\sigma_{60\%}$) and the ratio of $\sigma_{60\%}$ at 70°C and 20°C. According to table 1, increasing the temperature from 20°C to 70°C reduces the $\sigma_{60\%}$ by approximately 60%. When the temperature rises to 80°C, the tensile strength of some plastic materials decreases to approximately 50% of the room-temperature strength (Hiroe and Motoyoshi, 1996). A similar trend was found for the plastic film used in greenhouses.

Contact Analysis and Rolling Contact Experiments

Analysis Model

The contact analysis and rolling contact experiment were first conducted at room temperature (T = 20°C). The various contact stresses, and the rolling contact problems of elastic film sandwiched between two parallel cylinders, were provided by Johnson (1985). However, results for plastic film sandwiched between two orthogonal pipes have not been reported. Therefore, this study investigated the deformation and stress of plastic film by elastic-plastic contact analysis. Figure 8 shows the FEM mesh for the static contact model. Both pipes and the film were constructed from hexahedron elements with eight nodes. The modeled film and pipe meshes (with dimensions of 0.1 mm × 0.1 mm × 0.375 mm and 0.1 mm × 0.1 mm × 0.08 mm, respectively) contained approximately 1.5×10^5 elements. To confirm the accuracy of the mesh, the orthogonal contact of two elastic pipes was initially compared with the Hertzian contact stress. The two results coincided within 1% error. The analysis was encoded in Marc (2012, MSC Software Corp., Newport Beach, Cal.) using the sparse solver of the MultiFrontal method. The pipe and plastic film were assumed as an elastic body and an elasto-plastic body, respectively. The model dimensions in

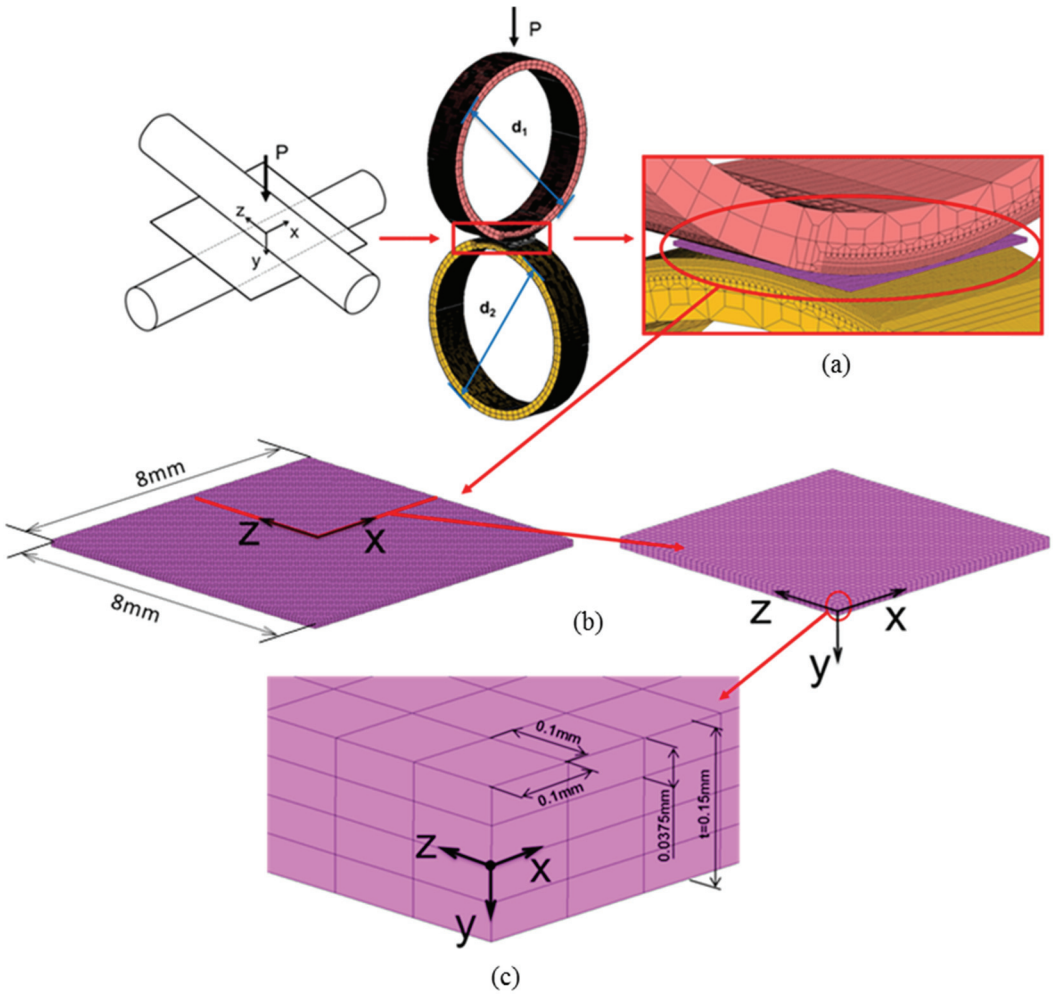

Figure 8. FEM mesh for static contact model of a single support pipe subjected to a load *P*: (a) 3D model for the plastic film between the two pipes. (b) mesh for FEM simulation of plastic film, and (c) dimensions of the film element are 0.1 mm × 0.1 mm × 0.0375 mm.

figure 8 are consistent with the actual dimensions of the open-roof greenhouse. The support and rolling pipes have the same outside diameter, $d_1 = d_2 = 38$ mm (inside diameter = 34 mm), and the plastic film is 0.15 mm thick (t_0 = 0.15 mm). Assuming that the rolling pipe weight is uniformly distributed over each support pipe, the average load on each support pipe is P = 15 N. Young's modulus and Poisson's ratio of the pipe are 210 GPa and 0.3, respectively. From the stress-strain diagrams in figures 7b and 7c, Young's modulus and Poisson's ratio of the plastic film (type A, B, C, and D) in the FEM analysis were derived as 450 MPa and 0.45, respectively. The boundary conditions are fixed displacements of the rolling pipe cross-section in the x and y directions and fixed displacements of the support pipe cross-section in the x, y, and z directions (fig. 8). The x, y, and z displacements are constrained at the origin (x, y, z) = (0, 0, 0) (fig. 8c).

Contact Stress and Deformation at Room Temperature

Figure 9 explains the contact state of type B film when P = 15 N, μ = 0, T = 20°C, and $d_1 = d_2$ = 38 mm. Figures 9a and 9b show the contact stress distribution. The contact stress (p_{max} = 7.14 MPa) is maximized at the center of the contact area. Figure 9c shows the boundary nodes between the contact and non-contact areas. The contact area is described by a circle (within the 5.1% error of the boundary nodes) where the radius of 0.88 mm is the average length from the origin. Figure 9d shows the profile of the thickness reduction. The contact area is circular when the support and rolling pipes have the same diameter.

Table 2 compares the stress and deformation in type B film at T = 20°C and T = 70°C. Other parameters were fixed as P = 15 N, μ = 0, and $d_1 = d_2$ = 38 mm. At 70° C, the maximum thickness reduction was twice that at 20°C, and the contact area was increased by 1.8. The results in table 2 were acquired for the same pipe diameters. The contact stress may be reduced by using a larger-diameter rolling pipe (Noda et al., 2015).

Table 2. Stress and deformation of type B film at different temperatures T (P = 15 N, μ = 0, and $d_1 = d_2$ = 38 mm.

	T = 20°C	T = 70°C
Maximum contact stress (p_{max}, MPa)	7.14	3.90
Contact length a (mm)	0.88	1.18
Contact length b (mm)	0.88	1.18
Contact area ($A_{contact} = \pi ab$, mm^2)	2.43	4.37
Maximum thickness reduction (Δt^{static}, mm)	0.020	0.038

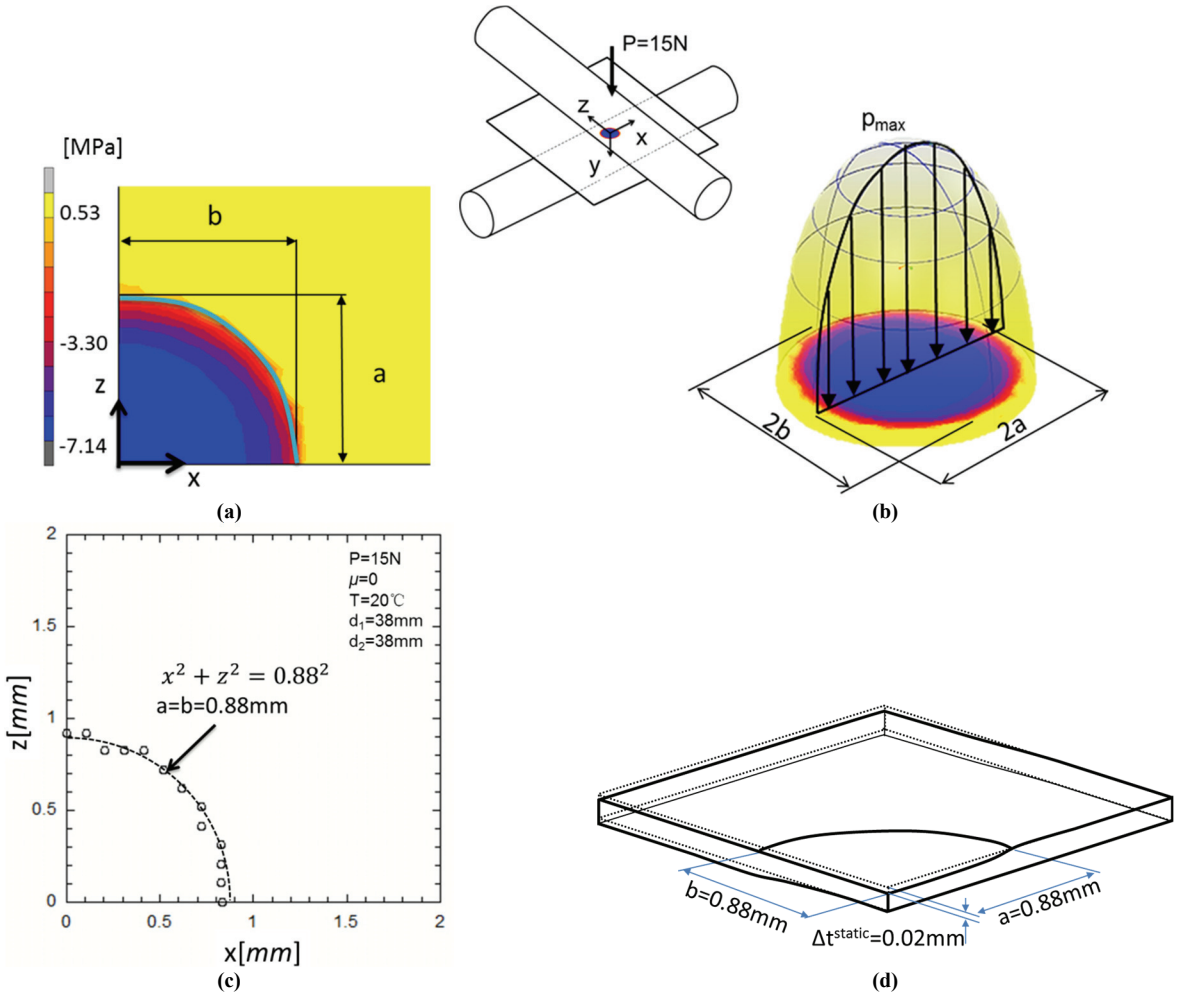

Figure 9. Stress and deformation of the film when P = 15 N, μ = 0, T = 20°C, and $d_1 = d_2$ = 38 mm: (a) stress σ_y at the contact area on the x-z plane, (b) maximum stress in the x-z plane is p_{max} = 7.14 MPa at the center of the plastic film, (c) contact area with dimensions $a = b$ = 0.88 (dotted line), and (d) thickness is maximally reduced at the center of the plastic film (Δt = 0.02 mm).

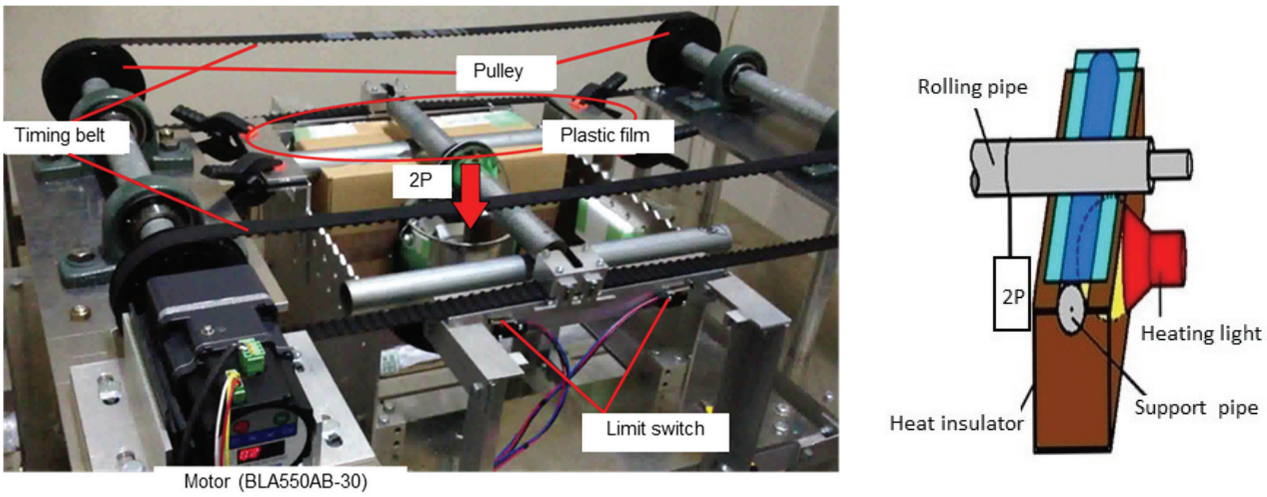

(a) (b)

Figure 10. (a) Rolling contact machine for investigating plastic film damage and (b) heated portion of support pipe with insulating box.

Rolling Contact Machine for Investigating Film Damage

The damage to greenhouse films caused by the roll-up movement was investigated with the apparatus shown in figure 10. Results were acquired for different plastic films, load magnitudes, temperatures, and pipe roughness. Each support pipe was subjected to a rolling contact load (P) within a stroke length of 25 cm. The plastic film was fixed at both ends of the support pipe. The speed of the rolling pipe was controlled from 30 to 750 mm min^{-1} by a brushless drive motor. In figure 10, the pipe that rolls over the film is pulled across and turns under the friction between itself and the film. The testing device in figure 10 differs from the greenhouse design in figure 1, where the film rolls around the moving pipe. In the testing device, a bare pipe is rolled over film that is laid over a support pipe. Therefore, unlike the greenhouse in figure 1, the rolling pipe rolls over the film and presses it onto the pipe beneath. The difference between figure 10 and figure 1 was investigated by comparing preliminary FEM results of a bare pipe and a film-wrapped rolling pipe. The film deformation was reduced in the latter case. It should be noted that in both figure 1 and figure 10, the line scar damage always occurred at the support pipe side of the film surface. Therefore, the line scars are similar for the bare pipe and film-wrapped pipe. By using the bare pipe, the appearance of line scars can be accelerated without changing the mechanism. Therefore, to prevent damage to the film, the rolling pipe or support pipe could be covered by a material with low elastic modulus.

Rolling Contact Experiments at Room Temperature

The rolling contact experiment was conducted in the rolling contact machine at room temperature. Fixing the stroke length at 20 cm, the numbers of line scars and creases were investigated while varying the load (P) and number of rolling cycles (N). The temperature was set to T = 20°C or T = 70°C, and $d_1 = d_2$ = 38 mm for plastic films of type A, B, C, and D. The load magnitude (P) ranged from 15 to 75 N. Although each support pipe carries an average load of 15 N, the actual load increases when the support pipe deflects. Greenhouse roofs are also subject to additional forces imposed by hard wind and rain and exerted by the holding strap (fig. 2). Therefore, we assumed that loads up to 75 N could be applied to the support pipe.

Table 3 lists the numbers of creases and line scars per centimeter in film type A examined at T = 20°C, N = 300, and $d_1 = d_2$ = 38 mm. A crease was determined in the following way. After the experiment, the film was placed on a black board and illuminated from above by a light source. The wave-like deformation captured by the reflected light was regarded as a crease. Results for other film types are excluded from table 3 because film type A exhibited the largest strain under the same stress (i.e., the lowest deformation resistance; fig. 7) among the tested films. The early stages of the study focused on film type B, which is used in the greenhouses of the Miyazaki Agricultural Research Institute. However, no line scars were detected on film type A at T = 20°C, as shown in table 3. Therefore, film type A, with the largest deformation, was adopted in later experiments. The Results and Discussion section will confirm that film type A has the largest thickness reduction Δt and the largest number of line scars ($n_{linescar}$ in table 8). Increasing the load on film type A increased the number of creases but induced no line scars at T = 20°C.

Table 4 shows the numbers of line scars and creases per centimeter in film type B when P = 15 N, T = 20°C, and $d_1 = d_2$ = 38 mm. As the number of rolling cycles increased from

Table 3. Number of creases and line scars per centimeter on film type A under different loads P (T = 20°C, N = 300, and $d_1 = d_2$ = 38 mm).

	P = 30 N	P = 60 N	P = 75 N
Number of creases per centimeter (n_{crease})	0.5	1.05	1.35
Number of line scars per centimeter ($n_{linescar}$)	0	0	0

Table 4. Number of creases and line scars per centimeter on film type B under different numbers of rolling cycles N (P = 15 N, T = 20°C, and $d_1 = d_2$ = 38 mm).

	N = 300	N = 1000
Number of creases per centimeter (n_{crease})	0.7	0.95
Number of line scars per centimeter ($n_{linescar}$)	0	0

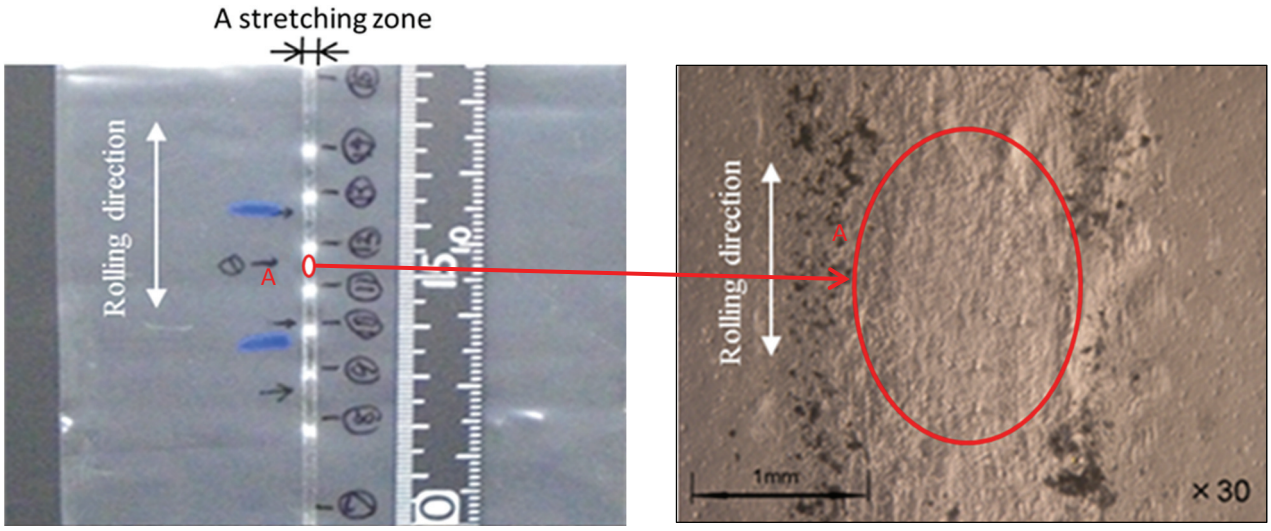

(a) (b)

Figure 11. Plastic film (type B) after rolling contact experiment. The white band is a stretched zone containing many creases but no line scars. Conditions are P = 15 N, T = 20°C, N = 300, and $d_1 = d_2$ = 38 mm: (a) rolling test piece and (b) enlarged view of test piece in the most severely damaged area.

N = 300 cycles to N = 1000 cycles, the number of creases (n_{crease}) increased by approximately 30%, but $n_{linescar}$ was 0 at T = 20°C.

Figure 11 shows the results of the rolling contact experiment. The white band shows the rolling indentation, where many creases occur. As shown in figure 11b, the largest damage appears at the center of the crease. This damage is due to the rough surface of the support pipe, but line scars, which should be perpendicular to the rolling direction, were not found. This result verifies that, despite the many creases, no line scars appear at 20°C.

Contact Stress and Deformation at T = 70°C

Although no line scars appeared at T = 20°C despite the many creases, they commonly occur in automatic ventilation greenhouses, where the temperature of the support pipe reaches 70°C in the summer. In other words, the damage is largely temperature-dependent. Therefore, the contact stress and deformation were investigated in detail at T = 70°C.

Table 5 shows the stress and deformation of film type B under different loads (P). Other parameters were fixed as μ = 0, T = 70°C, and $d_1 = d_2$ = 38 mm. Increasing the load by a factor of 5 (from P = 15 N to P = 75 N) increased the maximum contact stress (p_{max}) and contact area ($A_{contact} = \pi ab$) by factors of 1.8 and 2.3, respectively, and doubled the maximum thickness reduction. As shown in table 5, the maximum thickness reduction (Δt^{static}) at P = 15 N was only 44% of that at P = 75 N. Therefore, when investigating the effect of the friction coefficient (μ) on the stress and deformation of film type B, P was set to 75 N. The results (with T = 70°C and $d_1 = d_2$ = 38 mm) are summarized in table 6.

Table 5. Stress and deformation in film type B under different loads P (μ = 0, T = 70°C, and $d_1 = d_2$ = 38 mm).

	P = 15 N	P = 75 N
Maximum contact stress (p_{max}, MPa)	3.90	6.98
Contact length a (mm)	1.18	2.14
Contact length b (mm)	1.18	2.14
Contact area ($A_{contact} = \pi ab$, mm^2)	4.37	14.3
Maximum thickness reduction (Δt^{static}, mm)	0.038	0.086

The friction coefficient (μ) between plastic and metal materials ranges from 0.15 to 0.3 (Yamakuchi, 1981). To investigate its wide-range effects, the friction coefficient was varied from 0.15 to 0.6 in the present study. Figures 12a and 12b plot the maximum stress (p_{max}) and maximum thickness reduction (Δt^{static}), respectively, as functions of μ. As μ increased, p_{max} was found to increase while Δt^{static} decreased. The larger friction between the plastic film and pipe suppressed the slippage of the plastic film and constrained the contact area. Therefore, increasing the friction coefficient (μ) reduced the contact area and increased the contact stress.

Rolling Contact Experiments at T = 70°C

To investigate the rolling contact phenomena at 70°C using the apparatus shown in figure 10a, the support pipe was heated to 70°C with a heating lamp, similar to the sunlight that heats a real greenhouse. The lamp irradiated the bottom surface of the support pipe, and the heated portion of the support pipe was covered with an insulating box, as shown in figure 10b. The temperature of the support pipe was confirmed to vary within ±2°C along the 25 cm stroke length. The temperature was controlled by adjusting the distance between the support pipe and the heating lamp.

Table 6. Effect of friction coefficient (μ) on the deformation of film type B (P = 75 N, T = 70°C, and $d_1 = d_2$ = 38 mm).

	μ = 0.15	μ = 0.2	μ = 0.3	μ = 0.4	μ = 0.5	μ = 0.6
Maximum contact stress (p_{max}, MPa)	17.54	19.84	23.64	26.98	30.03	32.71
Contact length a (mm)	1.769	1.74	1.621	1.594	1.491	1.475
Contact length b (mm)	1.769	1.74	1.621	1.594	1.491	1.475
Contact area ($A_{contact} = \pi ab$, mm^2)	9.831	9.511	8.255	7.982	6.984	6.835
Maximum thickness reduction (Δt^{static}, mm)	0.0803	0.0749	0.0671	0.0615	0.0575	0.0539

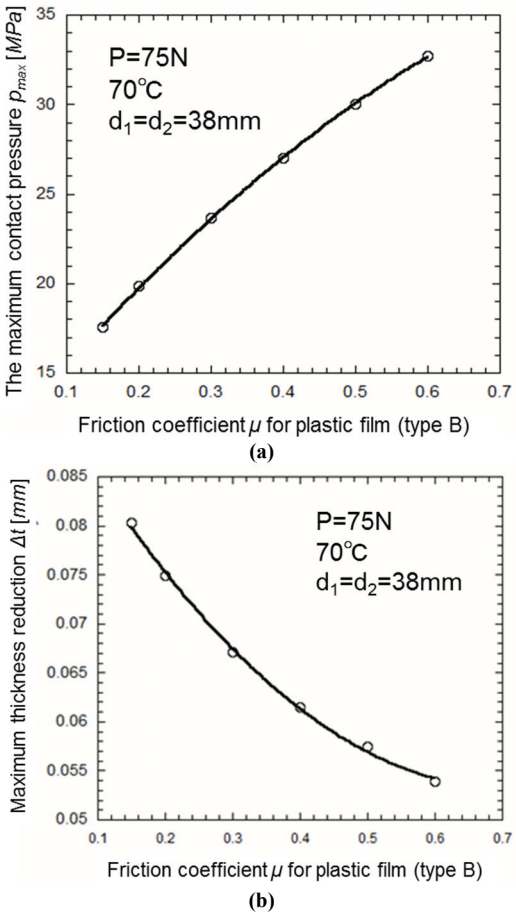

Figure 12. (a) Maximum contact pressure (p_{max}) and (b) maximum thickness reduction (Δt) as functions of the friction coefficient (μ). As μ increases, p_{max} increases while Δt decreases.

During the rolling contact experiments, the number of rolling cycles, pipe temperature, and load were set to 300, 70°C, and 75 N, respectively. Figure 13 shows the stretching zone of film type B by optical microscopy. Figure 14 is an SEM image of the inside of the damaged plastic (type B) film. Damage occurred at the support pipe side of the plastic film, mimicking the real damage in greenhouses (fig. 3b). In the close-up view (fig. 14b), a line scar is seen to have developed from creases that have folded over.

Results and Discussion

Analysis Model of Rolling Contact

The preceding sections presented the static contact analysis and discussed the maximum contact stress and maximum thickness reduction between the pipes. This section is devoted to the rolling action of the pipe, which occurs in actual automatically controlled greenhouse roofs. Therefore, it is necessary to compare the results of the static and rolling contact analyses.

Figure 15 illustrates the FEM mesh in the rolling contact analysis. Different from figure 8, the origin is situated on the support pipe side of the film surface. At the end of the film (x = -3.6 mm), the support pipe and all displacements in the x, y, and z directions are constrained. The pipe then rolls in the x direction, as shown in figure 15. In the perpendicular contact model, the support and rolling pipes have the same diameter ($d_1 = d_2$ = 38 mm). The number of elements is approximately 6.2×10^4, and the smallest mesh is 0.09 mm × 0.09 mm × 0.375 mm. Because Young's modulus of iron is approximately 420 times that of plastic film, the pipes were regarded as rigid bodies to simplify the model. The rolling speed and rolling time of the pipe in the FEM simulations were set to 8.38 rad min^{-1} and 1.3 s, respectively. As in the static contact analysis, the load magnitude was assumed as P = 75 N.

Results of Rolling Contact Analysis

Figure 16 shows the compressive strain distribution (ε_y) of film type B as the pipe rolls from its original point a to the finishing point d. Figure 17a shows the film thickness at x = 0, before the pipe started rolling. The initial film thickness (t_1) was 0.07 mm. The film thickness was minimized at x = 2.46 mm (t_2 = 0.04 mm); in other words, the maximum thickness reduction was Δt_2 = 0.15 − 0.04 = 0.11 mm at x = 2.46 mm. The film thickness was steady (t_3 = 0.06 mm) between x = 11.6 mm and x = 21.7 mm (fig. 17c). At x = 21.7 mm (the end of the rolling process), the film thickness (t_4) was 0.06 mm. In summary, the thickness reduction (Δt_2 = 0.11 mm) was maximized close to the start point of the rolling pipe, and thereafter became steady ($\Delta t_3 = \Delta t_4$ = 0.15 − 0.06 = 0.09 mm). Figure 18 schematizes the deformation of

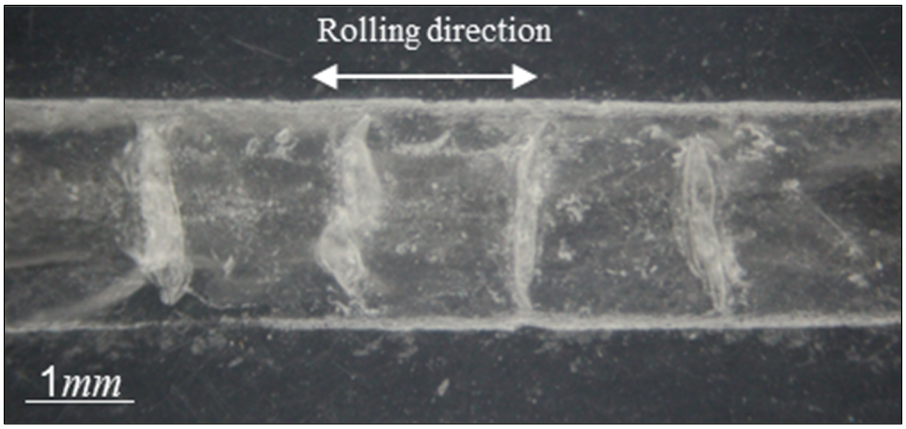

Figure 13. Microscopic white band indicates a stretching zone of film type B after N = 300 rolling cycles (P = 75 N, T = 70°C, and $d_1 = d_2$ = 38 mm). All four line scars are perpendicular to the rolling direction.

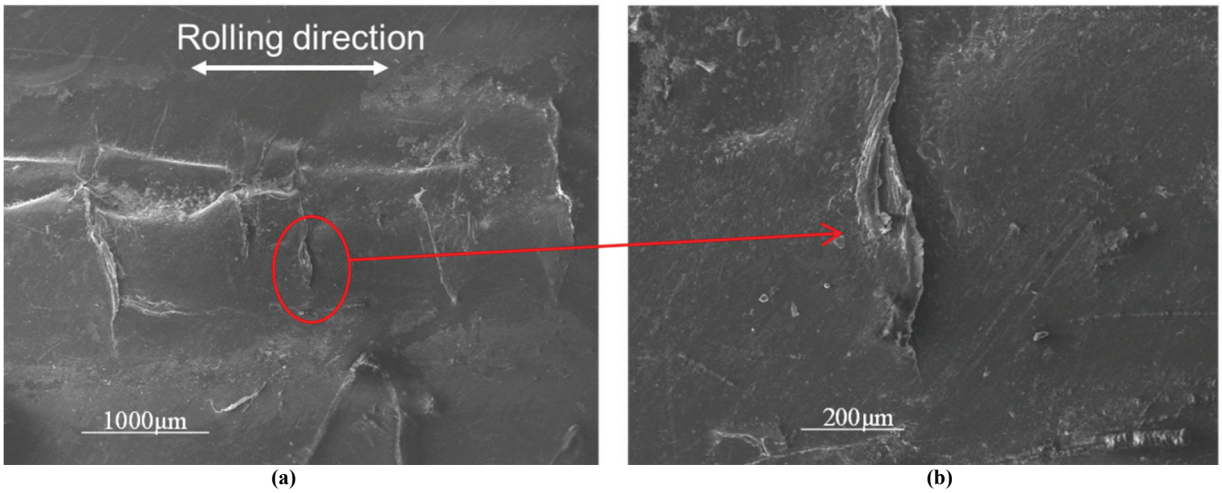

Figure 14. SEM images of damaged plastic film (type B) after N = 300 rolling cycles (P = 75 N, T = 70°C, and d_1 = d_2 = 38 mm): (a) line scars observed on the inside surface of the film and (b) close-up of a line scar.

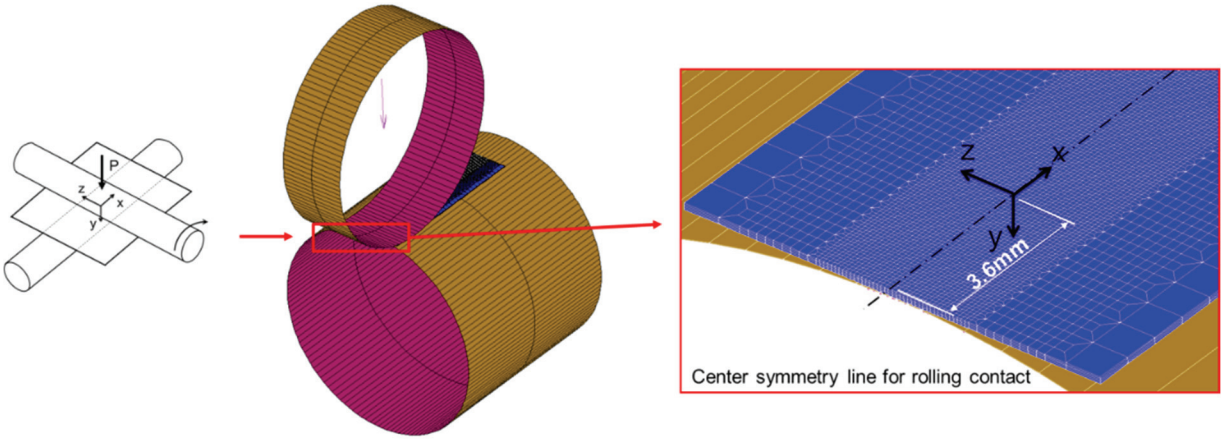

Figure 15. FEM mesh under rolling contact analysis.

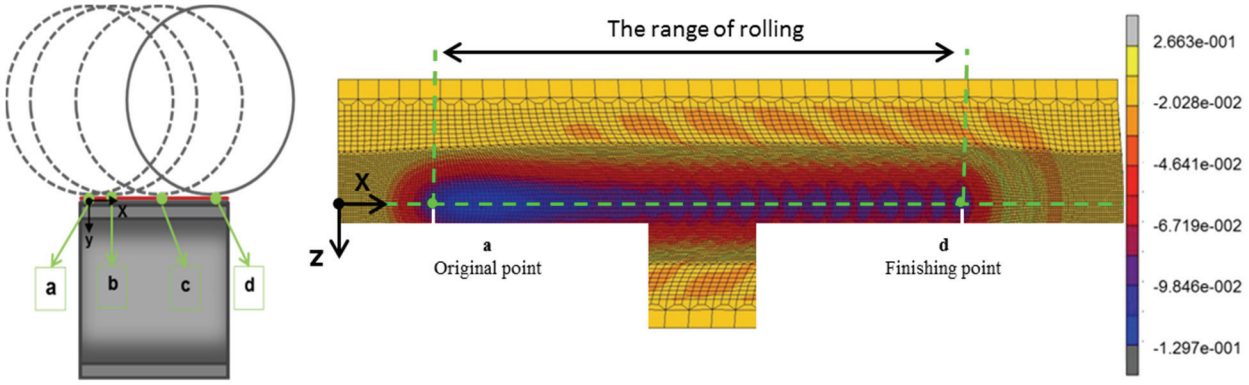

Figure 16. Strain distribution (ε_y) on film type B under rolling contact (P = 75 N, μ = 0.15, T = 70°C, and d_1 = d_2 = 38 mm).

film type B after the rolling pipe movement. The final thickness at most positions was 0.06 mm. Note that at the end of the film, the thickness increased to 0.18 mm due to the film extrusion by the rolling pipe. Figure 19 shows the deformation of film type B at different locations as the pipe rolled along the x direction. Deformations other than thickness reduction, such as frontal creases, are evident in this figure. The height of the frontal crease increased as the rolling pipe advanced. At x = 11.6 mm, the height became steady at h = 0.06 (that is, the thickness reduction stabilized at $\Delta t_3 = \Delta t_4$ = 0.09 mm). Under these steady-state conditions, the front of the rolling pipe was always preceded by two frontal creases, which might be largely responsible for the film damage. Figure 20 shows the thickness reduction, $\Delta t(x)^{rolling}$, of film type B under rolling contact along the length direction (x). Initially, the film was 0.15 mm thick. Here, the notations

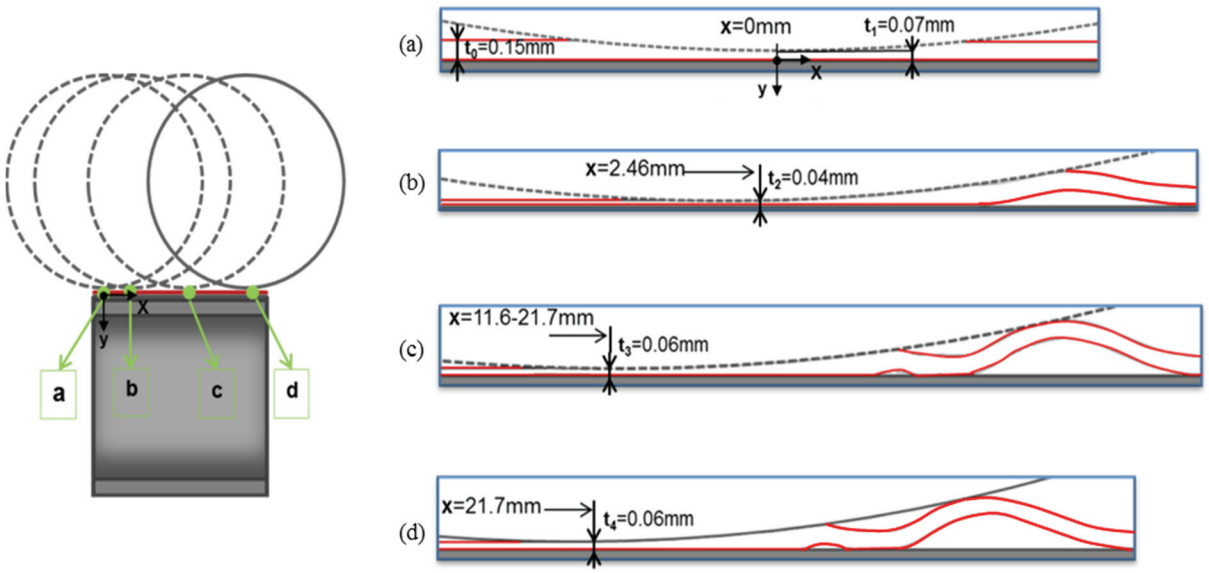

Figure 17. Thickness of film type B when P = 75 N, μ = 0.15, T = 70°C, and $d_1 = d_2$ = 38 mm: (a) static compression at x = 0, (b) maximum thickness reduction at x = 2.46 mm, (c) steady thickness reduction from x = 11.6 to x = 21.7 mm, and (d) final thickness reduction at x = 21.7 mm.

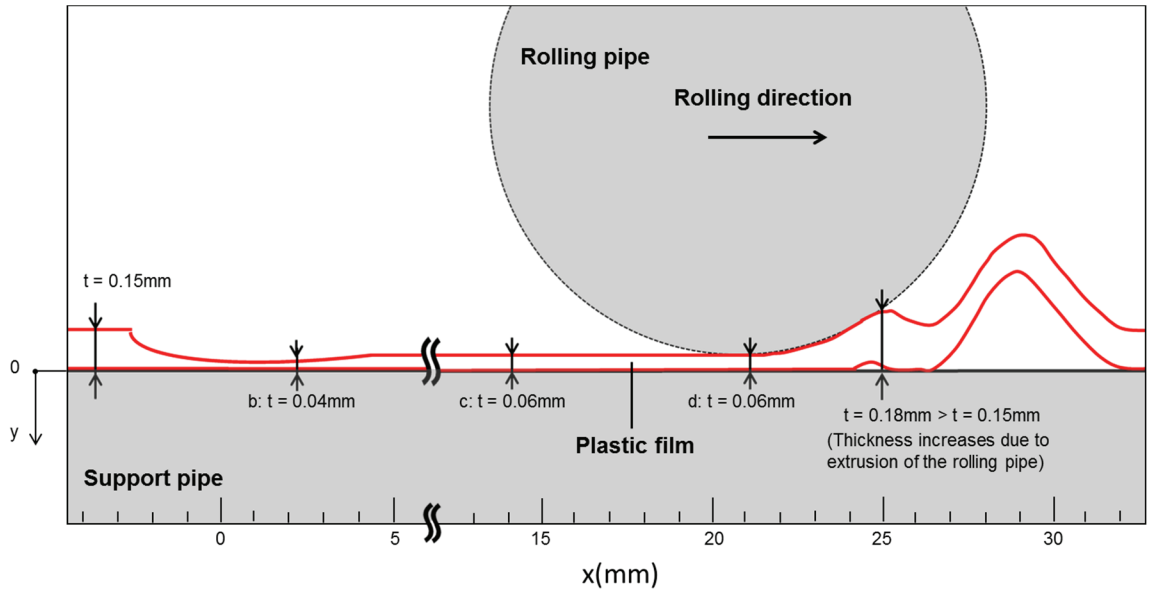

Figure 18. Schematic of deformation of film type B after rolling pipe movement.

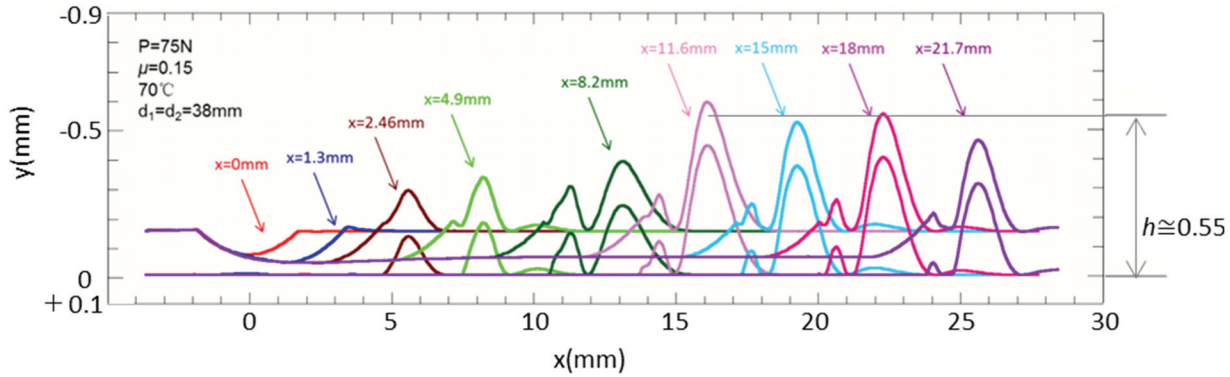

Figure 19. Growth of frontal crease height $h(x)$ of film type B at different x locations of the rolling pipe.

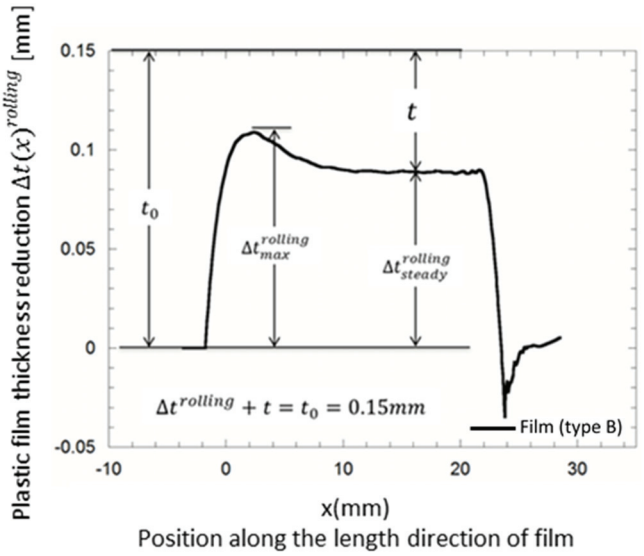

Figure 20. Plastic film thickness reduction ($\Delta t_{rolling}$) along the length direction of film type B (P = 75 N, μ = 0.15, T = 70°C, and d_1 = d_2 = 38 mm).

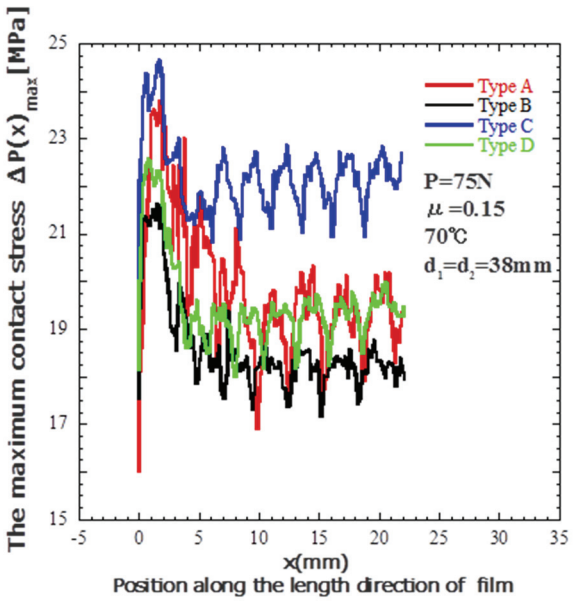

Figure 22. Maximum contact stress (p_{max}) on four kinds of plastic film along the length direction (P = 75 N, μ = 0.15, T = 70°C, and d_1 = d_2 = 38 mm).

$\Delta t(x)_{steady}^{rolling}$ and $\Delta t(x)_{\max}^{rolling}$ denote the steady-state and maximum thickness reductions, respectively, under the rolling contact, and $t(x)$ denotes the thickness of the plastic film. Note that the thickness reduction $\Delta t(x)_{steady}^{rolling}$ and the thickness $t(x)$ of the plastic film under rolling contact are related by $\Delta t(x)_{steady}^{rolling} + t(x) = t_0 = 0.15$ mm. Figure 21 shows the thickness reduction $\Delta t(x)_{steady}^{rolling}$ in the four kinds of plastic film. The thickness reduction was largest in film type A. The maximum contact stress on the film is plotted as a function of x in figure 22.

The rolling contact induced elongation and frontal creasing of the films. Figure 23 shows the deformations of the four films (type A, B, C, and D). The notations l and $\Delta l(x)$ denote the original length and the elongation in the x direction, respectively, and h denotes the frontal crease height. The obtained $\Delta l(x)$, h, and thickness reduction $\Delta t(x)_{steady}^{rolling}$ are summarized in table 7. Figures 24a and 24b plot the frontal crease height (h) and thickness reduction, respectively, as functions of the elongation in the rolling contact analysis with the approximate equation: $h = 0.11\Delta l_x + 7.0 \times 10^{-4}$ ($R^2 = 0.79$) and $\Delta t_{steady}^{rolling} = 0.015\Delta l_x + 0.031$ ($R^2 = 1.0$). The frontal crease height (h) increased with increasing elongation $\Delta l(x)$, while the thickness decreased. Only the central part of the rolling indentation elongated under the rolling; both sides of the rolling indentation were constrained. Therefore, the creases might develop from the stretched central portion of the film. Because crease formation is closely related to the elongation $\Delta l(x)$ and thickness reduction $\Delta t(x)_{steady}^{rolling}$, creases are considered as early damage preceding the formation of line scars.

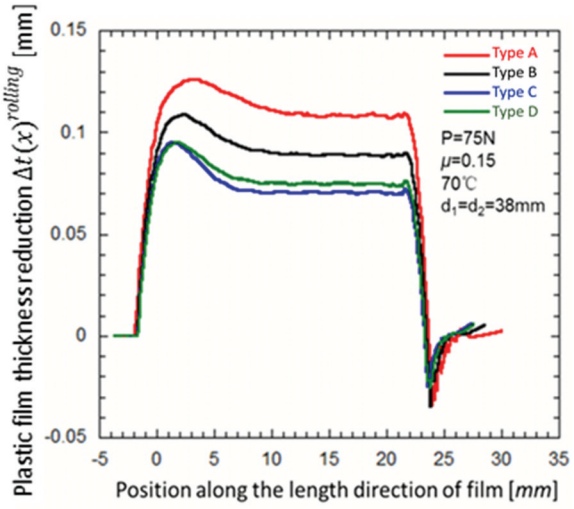

Figure 21. Thickness reduction ($\Delta t_{rolling}$) of four kinds of plastic film along the length direction (P = 75 N, μ = 0.15, T = 70°C, and d_1 = d_2 = 38 mm).

Comparison between Static and Rolling Contact Analyses

Figure 25 illustrates the three-dimensional deformation of film type B when P = 75 N, μ = 0.15, T = 70°C, and d_1 = d_2 = 38 mm. The frontal crease is accompanied by other creases at both sides of the stretched zone. The thickness reductions of film type B at z = 0 under static and rolling contact are compared in figure 26. Here, the notation Δt^{static} denotes the maximum thickness reduction under static contact, and $\Delta t_{steady}^{rolling}$ and $\Delta t_{\max}^{rolling}$ denote the steady-state and maximum thicknesses, respectively, under rolling contact. In both analyses, the thickness reduction was highest just after the original contact point.

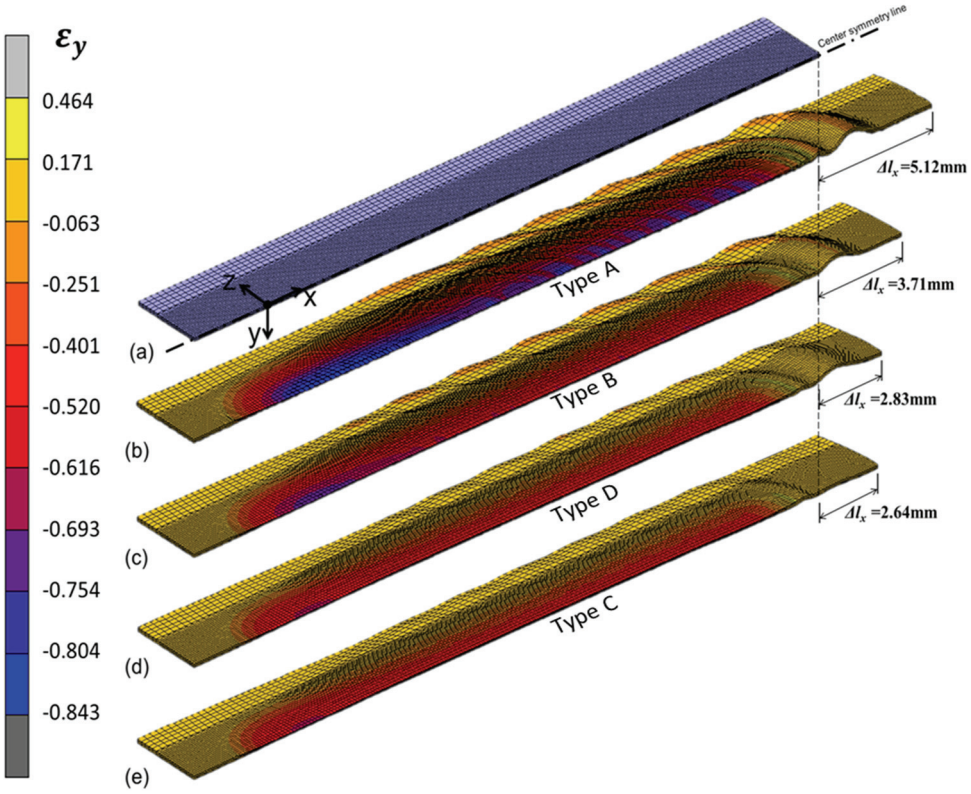

Figure 23. Strain distribution (ε_y) and deformation of (a) original plastic film and films of (b) type A, (c) type B, (d) type C, and (e) type D. Other parameters are P = 75 N, μ = 0.15, T = 70°C, and $d_1 = d_2$ = 38 mm.

Table 7. Elongation, thickness reduction, and frontal crease height of plastic films under rolling contact.

	Plastic Film Type			
	A	B	C	D
Elongation (Δl, mm)	5.12	3.71	2.64	2.83
Thickness reduction ($\Delta t_{steady}^{rolling}$, mm)	0.109	0.089	0.070	0.075
The frontal crease height (h, mm)	0.57	0.44	0.22	0.40

Next, the effect of the friction coefficient (μ) on the thickness reduction $\Delta t(x)^{rolling}$ was investigated under rolling contact. Figure 27 plots the thickness reduction of film type B obtained in the rolling contact analysis. The thickness reduction was a decreasing function of the friction coefficient. For six different friction coefficients, the thickness reductions Δt^{static}, $\Delta t_{steady}^{rolling}$, and $\Delta t_{\max}^{rolling}$ under static and rolling contact are plotted in figure 28. Again, in both static and rolling analyses, the thickness reduction decreased with increasing friction coefficient (μ).

Table 8 tabulates the thickness reductions in the four tested films. Comparing the results of the static and rolling contacts, we find that $\Delta t_{steady}^{rolling}$ was larger than or nearly equal to Δt^{static} for the four films.

Comparison between Rolling Contact Experiment and Contact Analysis

Table 8 presents the numbers of line scars ($n_{linescar}$) per centimeter observed during the rolling contact experiments

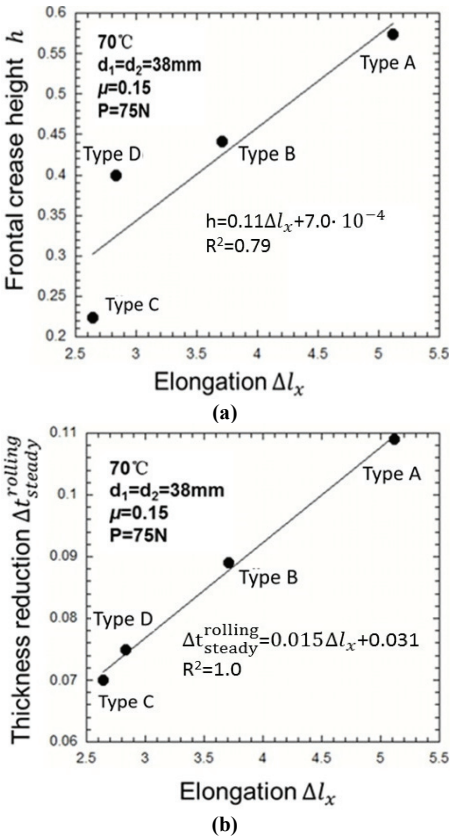

Figure 24. Relationship between (a) frontal crease height (h) and elongation (Δl_x) and (b) thickness reduction ($\Delta t_{steady}^{rolling}$) and elongation (Δl_x).

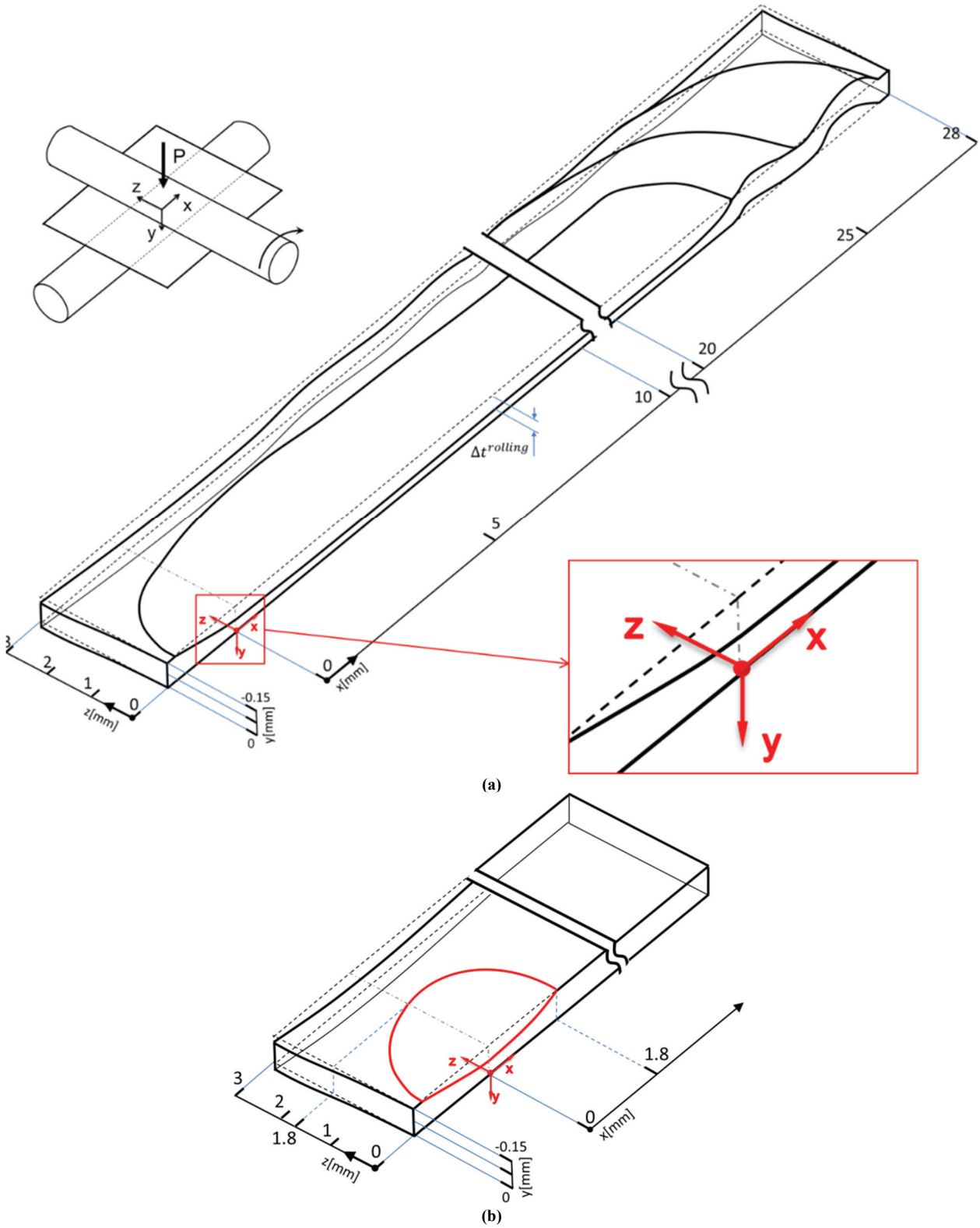

Figure 25. Deformation of plastic film (type B) when P = 75 N, μ = 0.15, T = 70°C, and d_1 = d_2 = 38 mm. Shown are the thickness reductions of the plastic film under (a) rolling contact analysis and (b) static contact analysis.

and the thickness reductions $\Delta t(x)^{rolling}$ obtained in the contact analysis with the approximate equation: $n_{linescar}$ = $202\Delta t^{static}$ – 13.9 (R^2 = 0.913) and $n_{linescar}$ = $108\,\Delta t^{rolling}_{steady}$ – 9.33 (R^2 = 0.849). The relationships between these two sets of results are plotted in figure 29. The number of line scars ($n_{linescar}$) was controlled by the two thickness reductions:

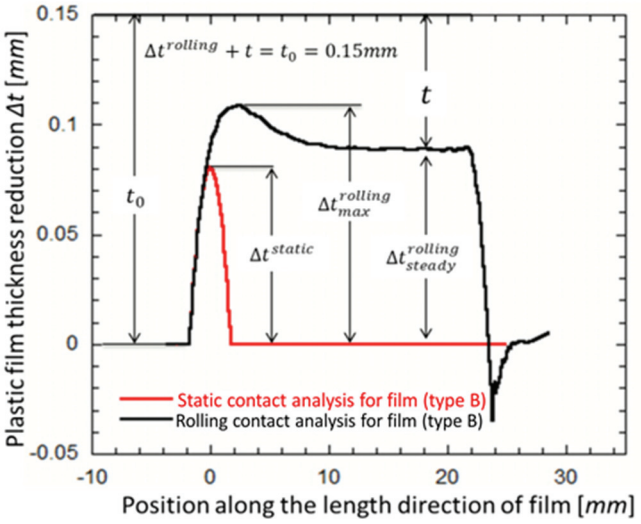

Figure 26. Thickness reduction of film type B along $z = 0$ in figure 25a. Red and black lines indicate the results of the static and rolling contact analyses, respectively.

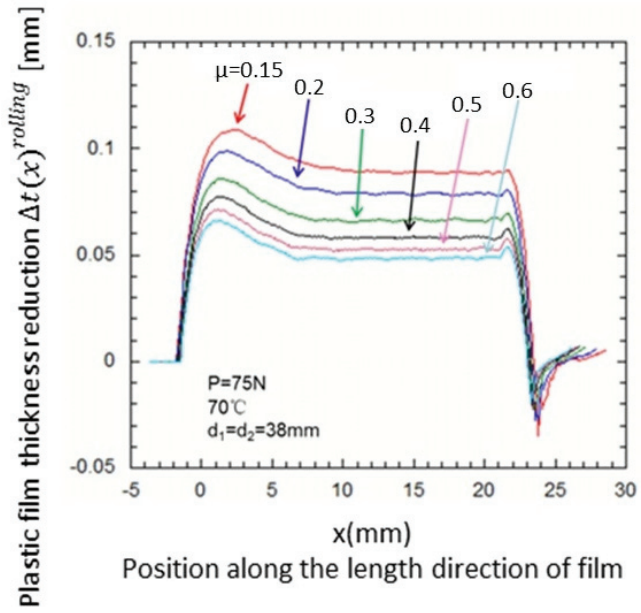

Figure 27. Thickness reduction of film type B versus friction coefficient μ ($P = 75$ N, $T = 70$°C, and $d_1 = d_2 = 38$ mm).

Δt^{static} and $\Delta t^{rolling}_{steady}$. In other words, reducing the film thickness increased the number of line scars per centimeter.

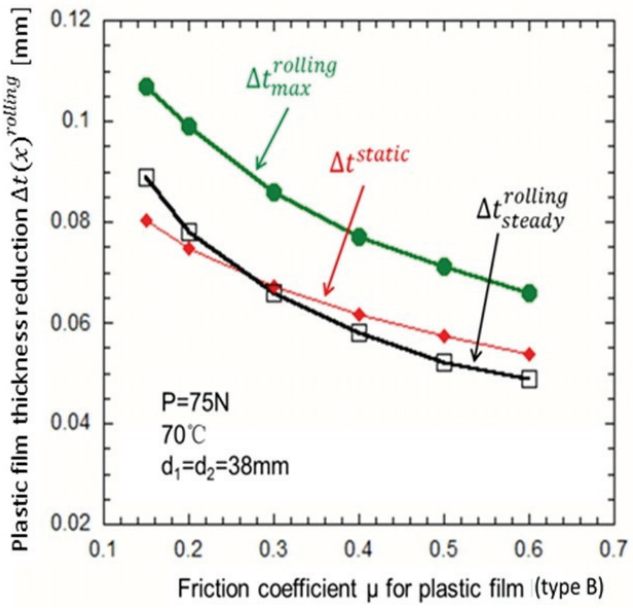

Figure 28. Effect of friction coefficient μ on Δt^{static}, $\Delta t^{rolling}_{steady}$, and $\Delta t^{rolling}_{max}$ defined in figure 26.

CONCLUSIONS

This study investigated the rolling contact damage in four types of plastic film used to cover automatically ventilated greenhouses. The mechanical damage under static and rolling contact was evaluated by finite element method (FEM) analysis. In addition, creases and line scars in the plastic film were generated by a newly designed rolling contact machine. The damage was also examined by microscopy techniques.

The results of the FEM analysis and rolling contact experiment are summarized below:

1. Microscopic observations of the outside and inside surfaces of real-world damaged films revealed that damage begins on the inside surface, which contacts the pipes of the greenhouse frame. The maximum roughness on the inside surface, as defined in JIS-B0601 (R_y = 11.6 μm), was approximately twice that on the outside surface (R_y = 5.1 μm).
2. The damage process can be summarized from these observations. Compressive rolling induces stretching zones that lead to creases. Eventually, the creases fold over and develop line scars perpendicular to the rolling

Table 8. Thickness reductions Δt^{static}, $\Delta t^{rolling}_{steady}$, $\Delta t^{rolling}_{max}$ and numbers of line scars per centimeter of plastic film under static and rolling contact analyses ($P = 75$ N, $\mu = 0.15$, $T = 70$°C, and $d_1 = d_2 = 38$ mm).

	Plastic Film			
	Type A	Type B	Type C	Type D
Maximum thickness reduction under static contact analysis (Δt^{static}, mm)	0.0897	0.0804	0.0744	0.0719
Thickness reduction in steady state under rolling contact analysis ($\Delta t^{rolling}_{steady}$, mm)	0.108	0.0889	0.0708	0.0748
Maximum thickness reduction under rolling contact analysis ($\Delta t^{rolling}_{max}$, mm)	0.125	0.107	0.0949	0.0947
$\Delta t^{rolling}_{steady} / \Delta t^{static}$	1.20	1.10	0.95	1.04
Number of line scars per centimeter ($n_{linescar}$)	3.85	2.95	1.2	0.15

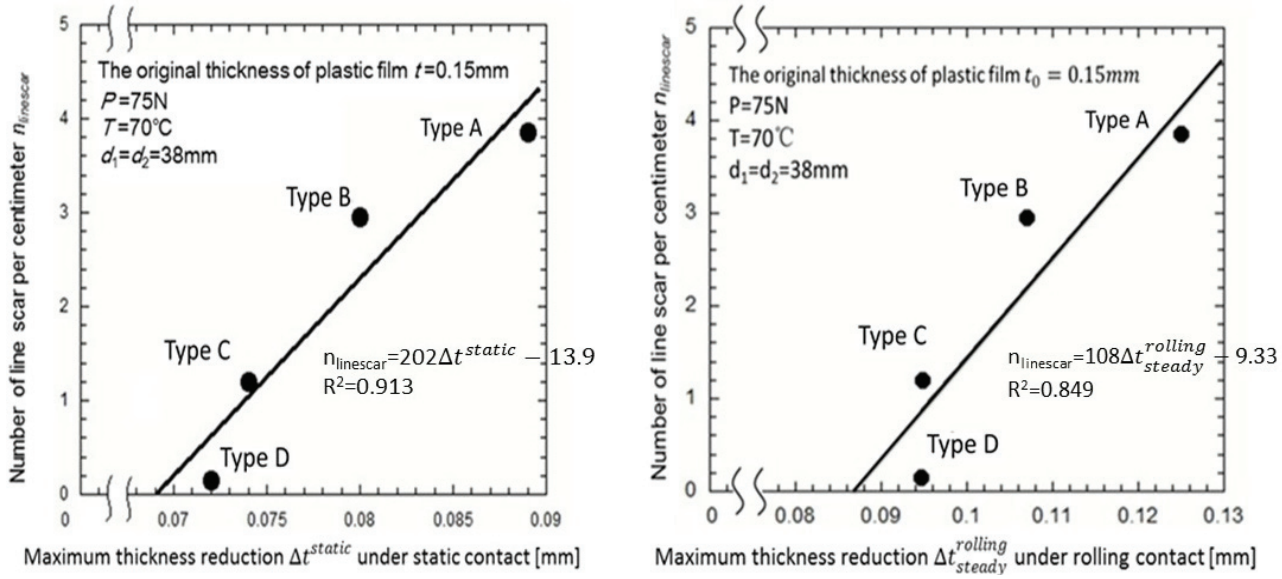

Figure 29. Number of line scars ($n_{linescar}$) per centimeter on four kinds of plastic films as an increasing function of (a) maximum thickness reduction Δt^{static} and (b) maximum thickness reduction $\Delta t_{steady}^{rolling}$.

direction. Finally, the plastic film breaks and splits.

3. In addition to reducing the film thickness, rolling contact caused elongation and creasing of the film. These deformations were closely related to film damage. The thickness was reduced the most just after the original contact point. The frontal crease height (h) increased as the rolling pipe progressed and stabilized at 11.6 mm from the start point (h = 0.06 mm), where the thickness reduction also became steady. The increased frontal crease height was associated with elongation and thinning of the film.
4. Friction between the plastic film and the pipe suppressed slippage of the film and prevented expansion of the contact area. Both effects contributed to maintaining the film's thickness. In other words, the friction coefficient largely affected the thickness reduction under both static loading and rolling contact.
5. The film damage was investigated with a novel rolling contact machine. The film supported by the pipes was repeatedly subjected to a rolling contact load. The type of plastic film, load magnitude, temperature, and number of rolling cycles were varied in these experiments. At room temperature, creases but no line scars were observed under any load or number of rolling cycles.
6. At 70°C (the measured maximum temperature of greenhouse pipes during the summer), the rolling contact experiment inflicted line scars on the plastic film. Thus, temperature severely influences the damage to plastic films. Creases and line scars are important damage processes, as described in conclusion 2.
7. The number of line scars was controlled by the thickness reduction under both static loading and rolling contact. The number of line scars on all films types increased with increasing thickness reduction.
8. It was found that film type D was the most suitable because line scars seldom appeared at temperatures under 70°C.

To maintain the film thickness under rolling contact, the pipe surfaces could be coated by a material with low elastic modulus. However, selecting the appropriate film and piping would increase the cost to greenhouse growers. Alternatively, the temperature damage could be reduced by selecting pipe materials that result in the lowest temperature rise under summertime sunlight heating.

ACKNOWLEDGEMENTS

The authors gratefully acknowledge Miyazaki Agricultural Research Institute for providing the plastic films and Nagatomo agricultural machinery for helpful discussions with this research. The authors also wish to express thanks to the members of their group, Mr. Yunpeng Huang, Mr. Yuki Hayashi, Mr. Qifeng Luo, Mr. Wanzhong Jiao, and Mr. Yigen Zuo, for their assistance in preparing the analysis data. The authors would like to thank Professor Hiroyuki Tanaka of the Kyusyu Institute of Technology for his kind support and advice regarding this collaborative study.

REFERENCES

Giacomelli, G. A., & Roberts, W. J. (1993). Greenhouse covering systems. *HortTech., 3*(1), 50-58.

Hiroe, S., & Motoyoshi, M. (1996). *Introduction to material properties of plastics.* Tokyo, Japan: Nikkan Kogyo Shimbun.

Japanese Industrial Standards. (1994). JIS-B0601: Geometrical Product Specifications (GPS)—Surface texture: Profile method—terms, definitions, and surface texture parameters. Tokyo, Japan: Japanese Industrial Standards Committee.

Japanese Industrial Standards. (1999). JIS-K7127: Testing method for tensile properties of plastic films and sheets. Tokyo, Japan: Japanese Industrial Standards Committee.

Japanese Industrial Standards. (2010). JIS-G3314: Hot-dip aluminum-coated steel sheet and strip. Tokyo, Japan: Japanese Industrial Standards Committee.

Johnson, K. L. (1985). *Contact mechanics.* Cambridge, UK: Cambridge University Press.

Miyazaki. (2012). Global warming countermeasure by Miyazaki Prefecture agricultural and fishery industries. Miyazaki Prefecture, Japan: Global Warming Research Center.
Nihon Nougyou System. (2014). Agricultural PO film. Tsuchiura, Japan: Nihon Nougyou System (Japan Agricultural System). Retrieved from www.nougyo-vinylhouse.com/po/
Noda, N.-A., Nagatomo, H., Luo, Q., Wang, L., Sano, Y., & Takase, Y. (2015). Rolling contact fatigue investigation and experimental simulation for plastic film used for full-opening and partially opening automatic ventilation greenhouses. Tokyo, Japan: Japan Society of Mechanical Engineers.
Sakaya, T., Nambu, J., & Kojima, T. (2005). Development of covering film for high-performance horticulture. *Sumitomo Kagaku, 2005-1*, 1-9. Retrieved from http://www.sumitomo-chem.co.jp/english/rd/report/theses/docs/20050102_pdo.pdf
Takakura, T. (1988). Protected cultivation in Japan. *Acta Hort., 230*, 29-38. http://dx.doi.org/10.17660/ActaHortic.1988.230.1
Tanimura, T., Hayashi, H., & Yamamoto, T. (2011). Dynamic tensile properties of plastic over a wide range of strain rates. *Trans. Japan Soc. Mech. Eng. Series A, 77*(780), 1347-1356. http://dx.doi.org/10.1299/kikaia.77.1347
Yamakuchi, S. (1981). *Lubricity of the plastic material: Application to the sliding portion and its characteristics.* Tokyo, Japan: Nikkan Kogyo Shimbun.